Optics and Laser Technology 112 (2019) 207–214

Contents lists available at ScienceDirect

Optics and Laser Technology

journal homepage: www.elsevier.com/locate/optlastec

Full length article

Optical analysis of nanostructured rose bengal thin films using Kramers–Kronig approach: New trend in laser power attenuation

M. Aslam Manthrammel[a], A.M. Aboraia[b,c], Mohd Shkir[a], I.S. Yahia[a,d,e,*], Mohammed A. Assiri[f], H.Y. Zahran[a,d,e], V. Ganesh[a], S. AlFaify[a], Alexander V. Soldatov[b]

[a] Advanced Functional Materials & Optoelectronic Laboratory (AFMOL), Department of Physics, Faculty of Science, King Khalid University, P.O. Box 9004, Abha, Saudi Arabia
[b] The Smart Materials Research Institute, Southern Federal University, Sladkova str. 178/24, Rostov-on-Don, Russia
[c] Department of Physics, Faculty of Science, Al-Azhar University, Assiut 71542, Egypt
[d] Research Center for Advanced Materials Science (RCAMS), King Khalid University, P.O. Box 9004, Abha 61413, Saudi Arabia
[e] Nanoscience Laboratory for Environmental and Bio-Medical Applications (NLEBA), Semiconductor Lab., Metallurgical Lab. 2 Physics Department, Faculty of Education, Ain Shams University, Roxy, 11757 Cairo, Egypt
[f] Advanced Materials and Green Chemistry Lab., Chemistry Department, Faculty of Science, King Khalid University, P.O. Box 9004, Abha, Saudi Arabia

HIGHLIGHTS

- Rose Bengal thin films were deposited on glass substrates with different thicknesses.
- Refractive and extinction indices values are calculated by Kramers-Kronig calculations.
- Third-order nonlinear optical susceptibility and refractive index values were estimated.
- Optical limiting is found to be enhanced by increasing the film thickness.
- Rose Bengal is a promising candidate for wide-scale optoelectronic applications and laser power attenuation.

ARTICLE INFO

Keywords:
Kramers–Kronig relations
Rose Bengal thin films
Linear/non-linear optics
Optical limiting of laser power

ABSTRACT

Highly stable Rose Bengal (RsB) organic semiconductor thin films were deposited on glass substrates with different thicknesses ranging from 95 to 325 nm. Optical transmission, reflection, and absorption studies were employed to analyze various optical constants. Refractive index and extinction coefficient values were attained using Kramers-Kronig calculations from the reflectance data. Dielectric constant, loss and dissipation factor were studied. Third-order nonlinear optical susceptibility and refractive index values were estimated using linear refractive index and absorption coefficient data for RsB films and studied their properties in nonlinear media. Optical limiting characteristics are found to be enhanced by increasing the thicknesses of films. The studied films can be used to limit the laser power of wavelengths 632 nm and 532 nm as an optical limiting material. The present work suggests that film of RsB is a promising candidate for wide-scale optoelectronic applications including IR pass filter, laser power attenuation, and selective CUT-OFF laser filters in the wavelength range 490–595 nm.

1. Introduction

Organic based thin films attract the researchers owing to their potential applications in device fabrications such as photovoltaic cells, FET, and LEDs [1–4]. Optical nonlinearities of organic-based thin films have attained special attention as high optical nonlinearity is considered to be a critical requirement in the next generation optical communication networks for realizing high speed and optical switching [5]. In particular, dye-based thin films have been achieving intensive interest in the recent past. Recently, many researchers including our team have reported the semiconducting nature of many dye-based thin films [6,7].

The aqua-soluble Rose Bengal (RsB) salt dye ($C_{20}H_2Cl_4I_4Na_2O_5$) is an anionic Xanthene derivative having the configuration 4,5,6,7-tetra-

* Corresponding author at: Advanced Functional Materials & Optoelectronic Laboratory (AFMOL), Department of Physics, Faculty of Science, King Khalid University, P.O. Box 9004, Abha, Saudi Arabia.
E-mail address: ihussein@kku.edu.sa (I.S. Yahia).

https://doi.org/10.1016/j.optlastec.2018.11.024
Received 29 June 2018; Received in revised form 20 August 2018; Accepted 10 November 2018
Available online 21 November 2018
0030-3992/

chloro-2′,4′,5′,7′-tetra-iodo-fluorescein disodium salt [8]. The first appearance of the RsB dye in the literature was reported in Schultz's tables, in 1881 [8,9]. It is also known as Acid Red 94, Bengal Rose B sodium salt and Rose Bengal sodium salt. Due to its robust absorption properties, RsB dye has found a significant part in numerous areas of medical, photochemistry and optical switching techniques [10,11]. Other people have tried RsB based thin films in poly(vinyl alcohol) (PVA) matrix and on FTO substrates, and have reported high stability of such films [12]. This films based on dyes are prepared by various techniques including spin coating, thermal evaporation, spray pyrolysis and chemical vapor deposition etc. [13].

In the present work, RsB dye based thin films with different thicknesses have been prepared on glass substrates using a spin coating method. Kramers-Kronig relations are used to estimate the refractive index and extinction coefficient for RsB thin films using reflectance data [14,15]. The linear and nonlinear optical properties were extracted using various models for optical thin films in some details.

2. Experimental details

2.1. Materials and deposition of RsB thin films on glass substrates

The Rose Bengal sodium salt dye was procured from Sigma-Aldrich. A 10^{-2} M RsB solution was prepared in 20 ml ethanol, mixed under magnetic stirring at room temperature and filtered well. This solution was housed inside a dark room to avoid interaction of light with it. Prior to deposition of films, substrates of glass were washed several times with soapy water followed by double distilled water and acetone solutions. At last, substrates were rinsed in water/isopropanol using the ultrasonic bath to get high quality cleaned substrates and then dried under nitrogen flow which ensures the absence of any contaminations. RsB thin films of various thicknesses were coated on glass substrates by varying the rotation speed of spin coater at 500, 1000, 2000 and 3000 rpm.

2.2. Devices and measurements

X-ray diffraction analysis for RsB-10B films were made by a Shimadzu XRD-6000 with CuK_α of wavelength $\lambda = 1.5406$ Å, at 30 mA and 30 kV. The measurements were made in the 2θ range from 10° to 70°. The surface morphology of RsB thin films was investigated by atomic force microscope (AFM) from (NT-MDT, Next (Russia)) and grain size and roughness were obtained by software attached to AFM device.

A JASCO V-570 UV–Vis– NIR spectrophotometer operated at normal incidence was employed to measure the absorbance $abs(\lambda)$, transmission $T(\lambda)$ and reflection $R(\lambda)$ of the RsB thin films at 300 K.

A Z-scan system with two lasers named as: He–Ne laser having wavelength 632.8 nm and input power = 371.5 μW was and Solid state green laser of wavelength 532 nm and input power = 18.84 mW were employed to investigate the optical limiting behavior of RsB films. The sample was fixed on the focal length of the lens. The samples were mounted on the laser beam path at the focal length of a lens which focuses the laser on film. The laser beam power with and without the sample was recorded using an optical power meter fixed at 632 nm and 532 nm.

An Alpha-Step IQ device profilometer was employed to measure the thin film thicknesses of RsB films on glass. The mean thickness values were calculated as 324, 259, 158 and 96 nm corresponding to the 500, 1000, 2000 and 3000 rpm of the spin coater, respectively.

3. Results and discussions

3.1. X-ray diffraction of RsB nanostructured thin films

Fig. 1a displays the X-ray diffraction patterns of different thicknesses RsB thin films. Films clearly display amorphous characteristics of all the synthesized thin films with the characteristic broad hump in the diffraction patterns [16]. From our previous work [17,18], we found that the amorphous nature of organic thin films supports the nanostructured of as-deposited organic films. Such discussions are based on the short-range order of amorphous materials. AFM image shows nanostructured films [Fig. 1b]

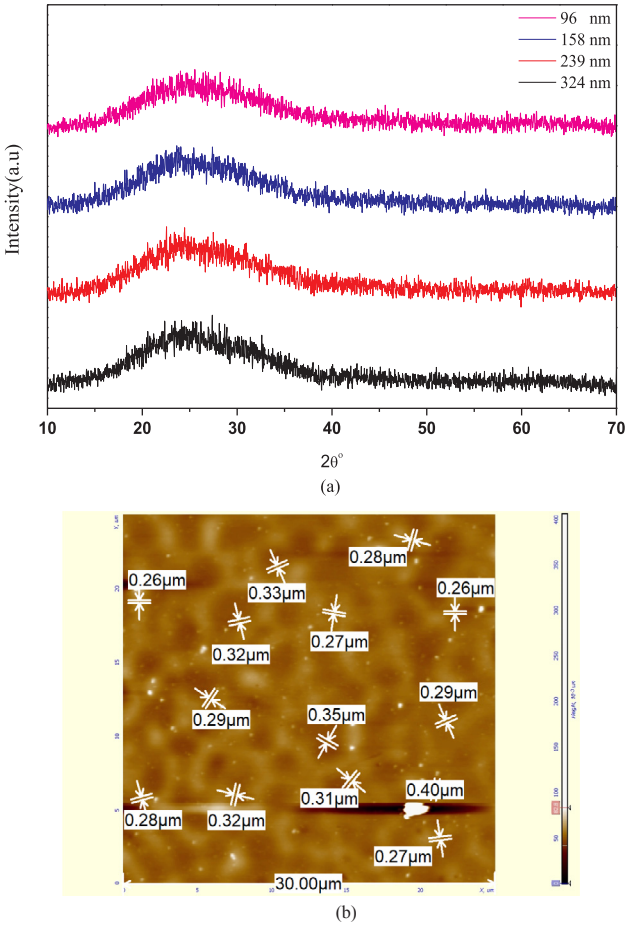

Fig. 1. (a) X-ray diffraction patterns and (b) AFM image of the RsB thin films.

3.2. Linear optics of RsB nanostructured thin films using Kramers-Kronig (K-K) relations

Extracting the optical constants accurately from the optical data such as transmission and reflection has always amused the research community and many techniques have been proposed which include Swanepoel's method [19], pointwise unconstrained minimization method [20,21]. Compared to these techniques, Kramers-Kronig relations is simpler, accurate and in the sense that the optical constants can be calculated just using the reflectance data alone without requiring detailed information regarding any kind of boundary conditions. That is, the K-K relations don't require any assumption or extrapolations of the reflectance experimental data which is beyond the measured range. The method is useful even when the measured data is limited within the narrow spectral range [22–24]. In the present study, Kramers-Kronig dispersion relations were employed to accurately calculate the optical constants (n and k) from the experimentally obtained reflectance data. The complex refractive index $N^{'}(\omega)$ has the form [25]:

$$N^{'}(\omega) = n(\omega) + ik(\omega) \quad (1)$$

where

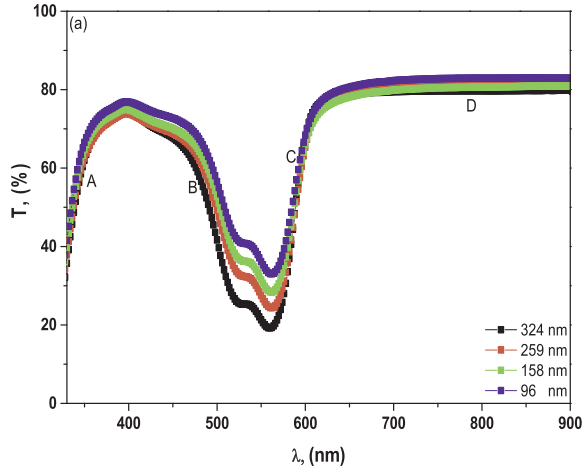

(a)

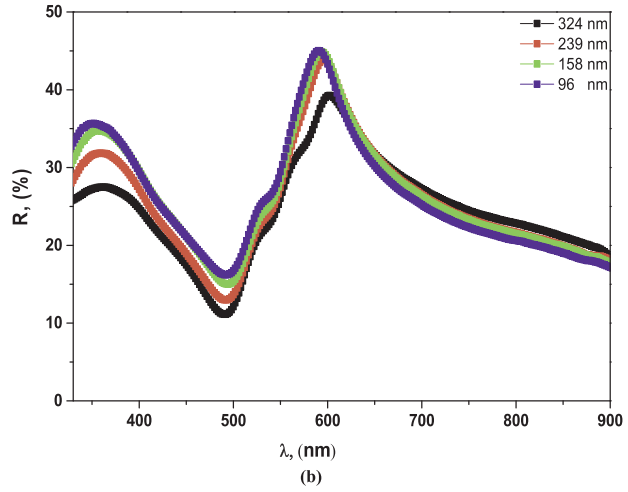

(b)

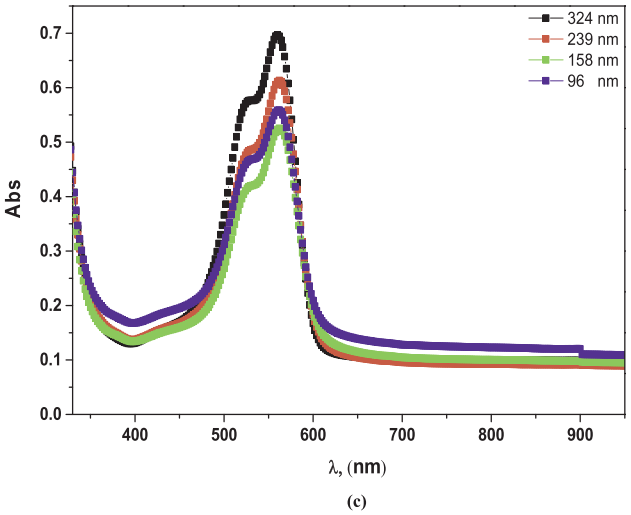

(c)

Fig. 2. (a-c). (a) Optical transmission, (b) reflection, (c) absorbance for RsB nanostructured thin films of different thicknesses.

$$n(\omega) = \frac{1 - R(\omega)}{1 + R(\omega) - 2cos\phi(\omega)\sqrt{R(\omega)}} \tag{2}$$

$$k(\omega) = \frac{1 - R(\omega)sin\phi(\omega)}{1 + R(\omega) - 2cos\phi(\omega)\sqrt{R(\omega)}} \tag{3}$$

and

$$\phi(\omega) = \frac{\omega}{\pi}\int_0^{\infty} \frac{\ln R(\omega') - \ln R(\omega)}{\omega^2 - \omega'^2} d\omega' \tag{4}$$

$$\Phi(\omega_j) = \frac{4\omega_j}{\pi}\Delta\omega \sum_i \frac{\ln(\sqrt{R(\omega)})}{\omega_i^2 - \omega_j^2} \tag{5}$$

Fig. 2(a-c) demonstrate the spectral behavior of optical transmission, $T(\lambda)$, reflection, $R(\lambda)$ and absorbance, $A(\lambda)$ at normal light incidence for the RsB thin films prepared at different thicknesses. From these spectra, it is very clear that a distinct absorption valley exists for the RsB thin films between 500 nm and 600 nm. From Fig. 2a, RSB thin films exhibit high transparency and bandpass filter characteristics in the NIR region above 620 nm and transmission declined sharply in the UV-region. Transmission spectra have the highest value of 82.9% in the NIR for the 96 nm thin film which gradually decreased to 79.8% for the 324 nm thin film. The absorption edges are observed to make systematic redshifts with film thickness, from 338 nm for 96 nm film to 342 nm for 324 nm thick RsB thin film. From transmission and absorption spectra, it is very evident that the films attenuate the transmitted light in the visible spectrum between 500 and 600 nm, in the absorption valley making the samples as a good choice for CUT-OFF laser filters in this range. The films exhibit maximum absorption in this range and a sharp increase in the reflection of light could also be observed for all the samples in the range (Fig. 2b). A systematic increase in the reflection is also observed with decreasing film thickness, below 600 nm wavelength which altered the order in the high transmission region > 600 nm. All the above discussions can support the same behavior for the absorbance data as shown in Fig. 2c. In absorption spectra, there are shoulder characteristics related to band valley of rose Bengal in the wavelength region from 512 to 539 nm.

Band gap, E_g for as-prepared thin films can be assessed from the absorption edge using the Tauc's relationship. In strong absorption region, the variation of absorption coefficient α is directly related to the occurrence of E_g and follows the relation [26–29]:

$$\alpha h\upsilon = A(h\upsilon - E_g)^m \tag{6}$$

where A is a constant, independent of energy and the index (m) is characteristics of the optical transition nature involved [30]. In our case, the optical data for the RsB thin films were best fitted with directly allowed transition corresponding to $m = 1/2$. Fig. 3 shows the Tauc's plots for the direct transition of all films. E_g values are attained from extrapolation of the linear part of $(\alpha h\upsilon)^2$ vs. $h\upsilon$ plot. E_g values are obtained at 1.924, 1.947, 1.954 and 1.979 eV corresponding to the film thicknesses 324, 259, 158 and 96 nm, respectively. The E_g of current RsB films is observed to be higher as well as compared with previously

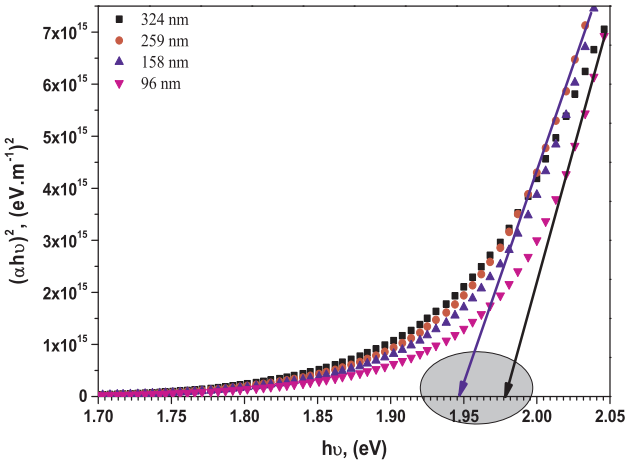

Fig. 3. Plots of $(\alpha h\upsilon)^2$ versus $h\upsilon$ for RsB thin films of different thicknesses.

Table 1
Comparative E_g and ε' and ε'' values for current and previously reported dyes.

Authors	*Materials*	*E_g (eV)*	ε'	ε''
Present work	*Rose Bingal*	*1.924–1.979*	-1 – 11 eV	-2 – 8 eV
Mohd Shkir et al. [J Mater Sci: Mater Electron (2017) 28:10573–10581]	Phenol red	*2.2*	4.8–23 eV	*0.6 – 8.5* eV
Abutalib et al. [Optik 127 (2016) 6601–6609]	Fluorescein dye	*1.95–1.99*	*2.7–4.9*	*0.05–1.1*
I.S. Yahia et al [PhysicaB490(2016)25–30]	*Rhodamine B*	*2.10*	*0.02–55*	—
El-Bashir et al., [Results in Physics 7 (2017) 1852–1858]	*Rose bengal/FTO*	—	*1–85*	*0.001–2*
El-Bashir et al., [Results in Physics 7 (2017) 1238–1244]	*PVA/ Rose bengal*	*3.923–1.838*	—	—

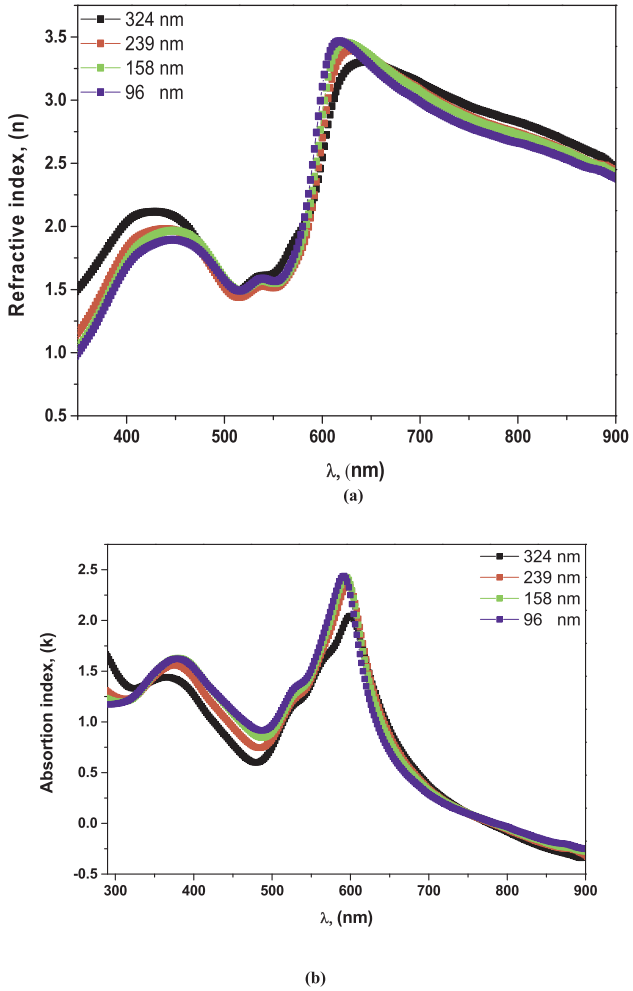

Fig. 4. (a&b). (a) Refractive index and (b) absorption index plots obtained from k-k calculations for RsB thin films of different thicknesses.

reported values for current as well as other dye systems (see Table 1). These band gap values are corresponding to the absorption edge wavelengths in the absorption valley range. The main absorption edge is thus attributed to the effect of strong absorption in the visible region of the Rose Bengal dye. The result indicates a blue shift in band gap values with reducing film thickness which could be attributed to nano growth of films [31].

Fig. 4(a & b) shows refractive index and absorption index plots in the range 330 to 900 nm obtained from Kramer-Kronig calculations for RsB thin films as-prepared at different thicknesses. From this figure, the refractive index spectrum displays a multi-oscillator behavior in this range due to multiple anomalous behaviors of the as-deposited thin films. The anomalous dispersion behaviors are observed in the ranges 270–420 nm, 515 nm -535 nm and 550–620 nm and could be ascribed to electron couplings in RsB thin films to the oscillating electric field generated from the resonance effect between the electron polarization and the light incident on the films [32]. The spectra display normal dispersion behaviors in the ranges 440–515 nm, 535–555 and above 620 nm which is the transparent region observed in Fig. 4a. The normal dispersion of the refractive index may be due to the single oscillator model. Also, it was noticed that the refractive index increases with film thickness.

Two main broad absorption bands could be observed in the *k*-spectra as shown in Fig. 4b, as follows: in the UV range centered at 375 nm and in the visible range around 590 nm, and both of bands are slight changes with RsB film thicknesses. The first one corresponds to the absorption shoulder while the other corresponds to the absorption valley. Also, it was noted that the absorption index trend with wavelength is almost analogous to that of the reflection spectrum and so, it showed the slight difference with a thickness below 350 nm and beyond 750 nm.

A complex dielectric function $\varepsilon = \varepsilon' + i\varepsilon''$ can be used to describe the optical response of any sample subjected to an incident electromagnetic radiation and defined as square othe f the complex the refractive index, $N = n + ik$ [33]. Thus,

$$\varepsilon' + i\varepsilon'' = [n + ik]^2 \quad (7)$$

Hence, the real and imaginary parts of dielectric functions, ε'&ε'' can be correlated with n and k as [34,35]:

$$\varepsilon' = n^2 - k^2 \quad (8)$$

$$\varepsilon'' = 2nk \quad (9)$$

The real component of dielectric constant, ε' effectively quantifies part of the stored energy which is proportional to the field amplitude and the imaginary component, ε'' describes the dielectric loss factor which is the portion of the electric energy that is lost through movement of ions/molecules as a result of the periodically varying field during the incident light interaction with the sample. Fig. 5a&b displays the of real and imaginary components (ε' and ε'') of dielectric constant versus wavelength plots in the in the range 330–900 nm, for RsB thin films. Absorption peaks for ε' are clear at 1.88, 2.31, 2.79 and 3.91 eV corresponding to 660, 538, 445 and 318 nm for the RsB of the film thickness = 248 nm. The ε' value for RsB films is comparable with previous reports on current as well as other dye systems (see Table 1). The trend of the graph with both the incident wavelength and film thickness is analogous to that of the refractive index spectrum. The graph displays the blue shift with film thickness a in lower wavelength region and red shift at the higher wavelength. Fig. 5b represents the spectral distribution of ε'' versus λ plots for RsB thin films. The graph showed absorption peaks at 2.04 and 3.16 eV corresponding to 610 and 393 nm of the film thickness = 248 nm. ε'' also displayed the blue shift of the broad peak in the lower wavelength side and red shift in the higher wavelength with the film thickness. The ε'' value for RsB films is comparable with previous reports on current as well as other dye systems (see Table 1).

Optical response of a thin film can be conveniently studied using optical and electrical conductivities (σ_{opt} and σ_e), respectively estimated from the experimentally obtained absorption coefficient (α). The optical conductivity is an overview of the electrical conductivity in the alternating field and strongly dependent on the free carriers allowed

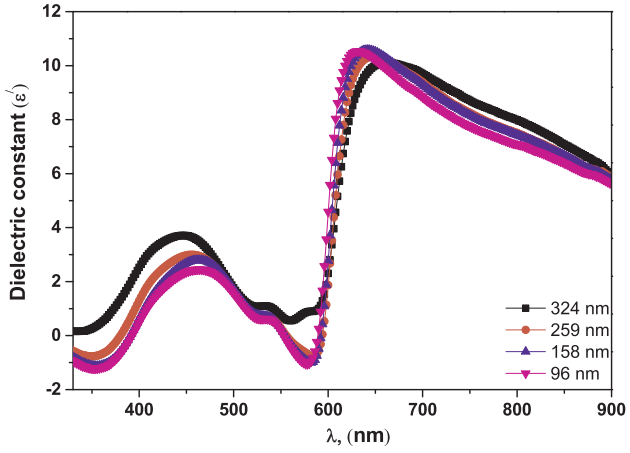

(a)

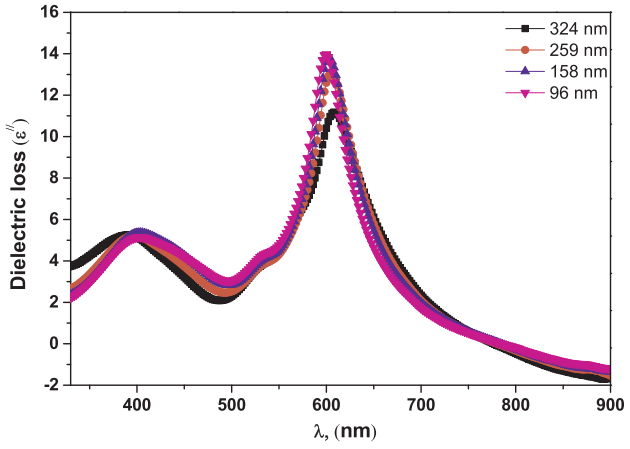

(b)

Fig. 5. (a,b). Spectral behaviors of $\varepsilon^{'}$ and $\varepsilon^{''}$ versus λ for RsB nanostructured thin films of different thicknesses.

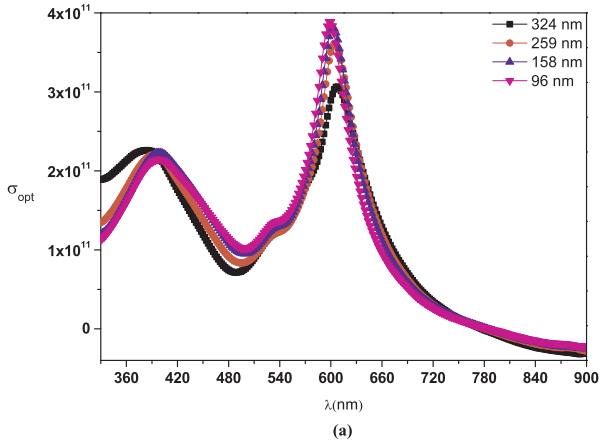

(a)

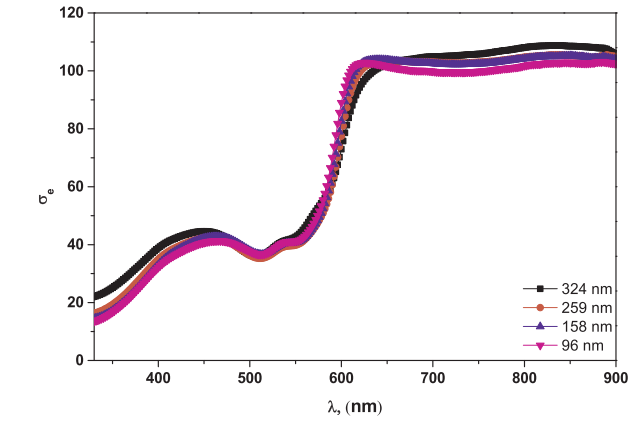

Fig. 6. (a,b). Spectral behaviors of the optical conductivity, and the electrical conductivity estimated from optical measurements for RsB thin films of different thicknesses.

interband transitions in the material [36,37]. The optical conductivity could be estimated from the relations [36,38,39]:

$$\sigma_{opt} = \alpha nc/4\pi \tag{10}$$

and

The electrical conductivity is related to the optical conductivity by the relation [38]:

$$\sigma_e = 2\lambda\sigma_{opt}/\alpha \tag{11}$$

where n and c are refractive index and light speed, respectively. Fig. 6(a,b) represent the spectral represents of optical and electrical conductivity versus wavelength for as-prepared RsB thin films of different thicknesses. From these figures, it is very clear that σ_{opt}plots exactly resemble that of $\varepsilon^{''}$ indicating the high dependence on the absorption coefficient of rose Bengal dye. Also two wide bands centered around ~ 395 and ~ 605 nm are observed in the Fig. 6a, which are corresponding to the absorption shoulder and absorption valley observed in the transmission/absorbance spectra. Due to the high absorption, more free carriers are available for conduction in these wavelengths. The optical conductivity decreases after the peak points as the incident photon energy decreases with increasing wavelength and thus, the excited free carriers available for conduction decreases. The valleys and negative points in the spectrum point out the trapping of the free carriers. Fig. 6b, displays the spectral behaviors of σ_e with respect to wavelength for all RsB thin films. From the graph, σ_e increases with the wavelength, accordan ince with the formula, $\sigma_e = \frac{2\lambda\sigma_{opt}}{\alpha} = 2\lambda nc/4\pi$. Moreover, as expected from the formula, the $\sigma_e$dependence on the film thickness analogous to the variation of refractive index as a functionthe of film thickness.

3.3. Nonlinear optics of RsB nanostructured thin films

Organic based thin films are a special class of optoelectronic materials with proven nonlinear optical (NLO) properties by which an applied electric field can modify the refractive index of the film. These properties are very useful in telecommunications, optical waveguides, and devices based on photorefractive effects [40]. The nonlinearity of optical susceptibility and optical polarizability (P) of thin films can be evaluated using [17,41]:

$$P = \chi^1 E + P_{nl}, \tag{12}$$

and

$$P_{nl} = \chi^2 E^2 + \chi^3 E^3, \tag{13}$$

where χ^1 and χ^3 are linear and third-order nonlinear optical susceptibilities, respectively [42]. Linear refractive index, $n(\lambda)$ can be evaluated using the below equation:

$$n(\lambda) = n_0(\lambda) + n_2(E^2) \tag{14}$$

where $(E)^2$ is the mean square of electric field [43]. In most cases, $n_0(\lambda) \gg n_2(\lambda)$, yielding $n(\lambda) = n_0(\lambda)$. The χ^1 and n are related by:

$$\chi^1 = \frac{{n_0}^2 - 1}{4\pi} \tag{15}$$

Also, χ^3 and χ^1 are related by the simple relation:

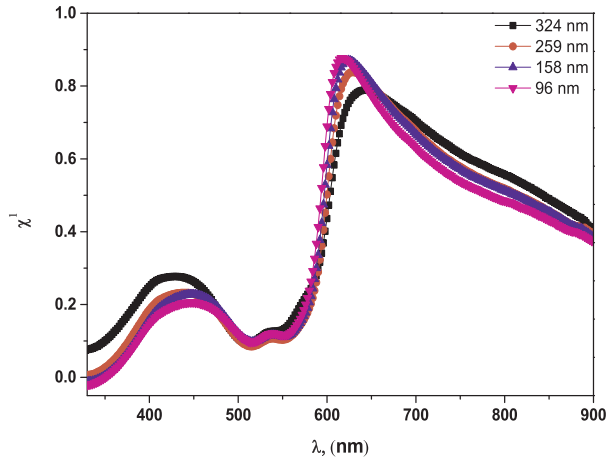

(a)

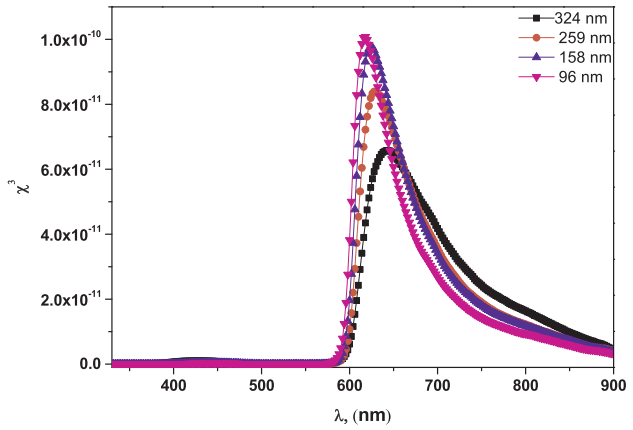

(b)

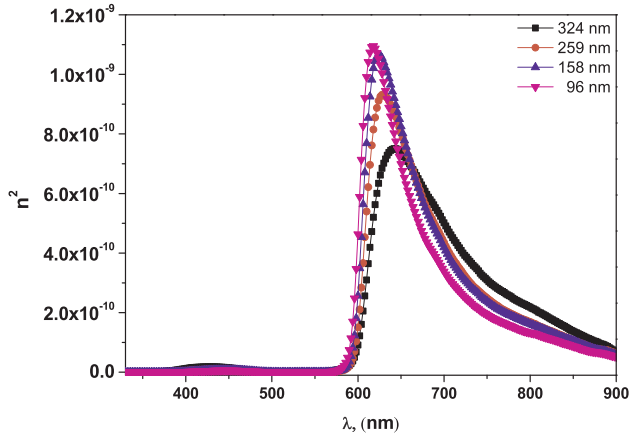

(c)

Fig. 7. (a-c). (a) linear optical susceptibility, $\chi^{(1)}$, (b) third-order nonlinear optical susceptibility, $\chi^{(3)}$ and (c) nonlinear refractive index, n_2 vs. wavelength plots for the RsB thin films.

$$\chi^3 = A.\ (\chi^1)^4, \tag{16}$$

implying,

$$\chi 3 = A(4\pi)^{-4}(n_0^2 - 1)^4, \tag{17}$$

where $A = 1.7 \times 10^{-10}$ esu is a constant [44,45]. Fig. 7 (a,b) represent the plots of linear and third-order nonlinear optical susceptibilities, χ^1, χ^3 with respect to the wavelength for RsB thin films. The plot of χ^1 closely resembles that of $\varepsilon^{'}$ except in the absorption valley range between 500 nm and 600 nm and suggests a strong relation between them. From the graph, the χ^1 values are found varying between -0.015 and 0.877 and 0.028 and 0.787 for the 96 nm thin film and 324 nm thin films, respectively, while the other films with the intermediate thicknesses followed the intermediate values. The value of χ^1 is found varying between -0.026 and 0.877 while that of χ^3 is found varying between $4x10^{-15}$ and 1.01×10^{-10}, with wavelength. Also, the value of χ^3 is found increasing with decreasing film thickness while that of χ^1 followed a mixed pattern. The value of χ^1 increased with the film thickness in the wave length ranges below 500 nm and beyond 600 nm while displaying the opposite trend in between wavelength range. The plot of nonlinear refractive index n^2 for RsB thin films as a function of wavelength is depicted in Fig. 7(c). The nonlinear refractive index can give significant information regarding the light gathering capacity of the film and thus considered as a very important parameter while studying the nonlinear behavior of a sample. The nonlinear refractive index, n^2 and χ^3 are related by [46,47]:

$$n^2 = \frac{12\pi\chi^3}{n_0} \tag{19}$$

From the figure, the value of n_2 is varying between $2x10^{-15}$ and $1.95x10^{-9}$. It was also noticed that the n_2 value decreases with film thickness and plot of n_2 is closely analogous to that of χ^3 and validates their strong dependence. The values of χ^1, χ^3 and n_2 for currently prepared RsB films are observed to be comparable with previous reports on current as well as other dye systems (see Table 2).

3.4. Optical limiting analysis of RsB /glass thin films

The optical limiting study is one of the key characteristics of optical materials which make them suitable for laser devices and human eyes. Hence, the optical limiting investigation has been carried out on the deposited films using two lasers of wavelengths 632.8 and 532 nm and effect of thickness have been studied. The optical limiting data from both lasers have been provided in Table 3. It can be seen that the output saturated power from both lasers is decreasing with the increase of the thickness of the films. This shows that thickness is playing a vital role in modifying the optical limiting behavior of RsB. As the limiting effect of the films is enriched, the possible reason it may be the higher thickness films possess a large number of molecules to compare to lower thickness films and hence they are taking part at large scale during the processing of nonlinear absorption [48,49]. Hence, the higher thickness films showing sturdy optical limiting characteristics and will be more applicable to laser devices.

4. Conclusions

Successful fabrication of Rose Bengal (RsB) nanostructured thin films was carried out on a glass substrate with different thickness using spin coating technique for the first time in literature. A robust investigation has been done on key characteristics of RsB thin films affected by thickness. Optical measurements were carried out to study various linear and nonlinear properties of RsB thin films. The refractive index and extinction coefficient was accurately estimated using Kramers–Kronig relations. Non-linear susceptibility and nonlinear refractive index studies were made on the principles of linear refractive index dispersion. Optical limiting behavior was studied using 632.8 and 532 nm lasers and the strong effect of thickness was observed. High transmission, IR bandpass and selective band stop filter and optical limiting characteristics make the RsB thin films a suitable semiconductor competitor for many optoelectronic applications.

Table 2
Comparative $\chi^{(1)}$ and $\chi^{(2)}$, $n^{(2)}$ values for current and previously reported dyes.

Authors	Materials	$\chi^{(1)}$	$\chi^{(3)}$, (esu)	$n^{(2)}$, (esu)
Present work	Rose Bingal	*0.026–0.877*	0.00004–1.01 ($\times 10^{-10}$)	0.000002–1.95 ($\times 10^{-9}$)
Mohd Shkir et al. [J Mater Sci: Mater Electron (2017) 28:10573–10581]	Phenol red	0.3–1.8	0.0089 – 1.55 ($\times 10^{-9}$) esu	0.003 – 1.22 ($\times 10^{-8}$ esu)
Abutalib et al. [Optik 127 (2016) 6601–6609]	Fluorescein dye	*1.88–2.25*	*0.15–0.32 esu*	*0.10 – 1.8 ($\times 10^{-12}$)*
I.S. Yahia et al [PhysicaB490(2016)25–30]	*Rhodamine B*	*0.1– 4*	*0.0001– 4.9* ($\times 10^{-8}$) esu	*0.0001– 2.3 ($\times 10^{-12}$)*
El-Bashir et al., [Results in Physics 7 (2017) 1852–1858]	*Rose bengal/FTO*	*0.05–7*	*4 $\times 10^{-7}$*	*1.6 $\times 10^{-6}$*
El-Bashir et al., [Results in Physics 7 (2017) 1238–1244]	*PVA/ Rose bengal*	*0.05–7*	*4 $\times 10^{-7}$*	*1.6 $\times 10^{-6}$*

Table 3
Optical limiting parameters for RsB films of different thicknesses using two different laser sources.

The input Intensity of (I_o)	For He-Ne laser at 632.8 nm I_o = 371.5 μW		For green laser at 532 nm I_o = 15.84 mW	
Samples / Thickness (nm)	Output power (μW)	Normalized power = output power/input power	Output power (mW)	Normalized power = output power/input power
324	276	0.743	9.292	0.587
239	287.4	0.774	9.311	0.589
158	286.1	0.770	10.84	0.684
96	307.6	0.828	10.54	0.559

Acknowledgment

The authors express their appreciation to "The Research Center for Advanced Materials Science (RCAMS)" at King Khalid University for funding this work under grant number RCAMS/KKU/003-18.

References

[1] C.W. Tang, S.A. VanSlyke, Organic electroluminescent diodes, Appl. Phys. Lett. 51 (1987) 913–915.
[2] A. Wada, J.-I. Nishida, M.M. Maitani, Y. Wada, Y. Yamashita, Dye-sensitized Solar Cells Based on 1,3-Dithiol-2-ylidene Derivatives: Substituent and π-Spacer Effects on the Efficiency, Chem. Lett. 43 (2013) 296–298.
[3] Q. Zhou, Q. Hou, L. Zheng, X. Deng, G. Yu, Y. Cao, Fluorene-based low band-gap copolymers for high performance photovoltaic devices, Appl. Phys. Lett. 84 (2004) 1653–1655.
[4] F. Garnier, R. Hajlaoui, A. Yassar, P. Srivastava, All-polymer field-effect transistor realized by printing techniques, Science 265 (1994) 1684.
[5] N. Junpei, K. Osamu, K. Takashi, S. YongGu, Fabrication of cyanine dye thin films grown by a layer-by-layer method, Mater. Res. Exp. 2 (2015) 076402.
[6] A. Bouzidi, I.S. Yahia, W. Jilani, S.M. El-Bashir, S. AlFaify, H. Algarni, H. Guermazi, Electronic conduction mechanism and optical spectroscopy of Indigo carmine as novel organic semiconductors, Opt. Quant. Electron. 50 (2018) 176.
[7] V. Ganesh, M.A. Manthrammel, M. Shkir, I.S. Yahia, H.Y. Zahran, F. Yakuphanoglu, S. AlFaify, Organic semiconductor photodiode based on indigo carmine/n-Si for optoelectronic applications, Appl. Phys. A 124 (2018) 424.
[8] D. Xu, D.C. Neckers, Aggregation of rose bengal molecules in solution, J. Photochem. Photobiol., A 40 (1987) 361–370.
[9] D.C. Neckers, The Indian happiness wart in the development of photodynamic action, J. Chem. Educ. 64 (1987) 649.
[10] V.K. Gupta, A. Mittal, D. Jhare, J. Mittal, Batch and bulk removal of hazardous colouring agent Rose Bengal by adsorption techniques using bottom ash as adsorbent, Rsc Adv 2 (2012) 8381–8389.
[11] C. Åkerlind, H. Arwin, F.L.E. Jakobsson, H. Kariis, K. Järrendahl, Optical properties and switching of a Rose Bengal derivative: a spectroscopic ellipsometry study, Thin Solid Films 519 (2011) 3582–3586.
[12] A.A. Abdel-Fattah, E.-S.A. Hegazy, M.A. El-Ahdal, H. Ezz-El-Din, Thin film dosimeters based on Rose Bengal dyed poly(vinyl alcohol), International Journal of Polymeric Materials and Polymeric, Biomaterials 51 (2002) 413–427.
[13] A.S. Radwan, M.M. Makhlouf, E. Abdel-Latif, Azothiophene dyes nanotubes structure based thin films: Synthesis, structural and optical characterization toward application in dye-sensitized solar cells, Dyes Pigments 134 (2016) 516–525.
[14] J. Mobley, K.R. Waters, M.S. Hughes, C.S. Hall, J.N. Marsh, G.H. Brandenburger, J.G. Miller, Kramers-Kronig relations applied to finite bandwidth data from suspensions of encapsulated microbubbles, J. Acoust. Soc. America 108 (2000) 2091–2106.
[15] J.E. Nestell, R.W. Christy, Derivation of optical constants of metals from thin-film measurements at oblique incidence, Appl. Opt. 11 (1972) 643–651.
[16] M.A. Zeeshan, D. Esque-de Los Ojos, P. Castro-Hartmann, M. Guerrero, J. Nogues, S. Surinach, M.D. Baro, B.J. Nelson, S. Pane, E. Pellicer, J. Sort, Electrochemically synthesized amorphous and crystalline nanowires: dissimilar nanomechanical behavior in comparison with homologous flat films, Nanoscale 8 (2016) 1344–1351.
[17] M. Shkir, V. Ganesh, S. AlFaify, I.S. Yahia, Structural, linear and third order nonlinear optical properties of drop casting deposited high quality nanocrystalline phenol red thin films, J. Mater. Sci.: Mater. Electron. 28 (2017) 10573–10581.
[18] M. El-Nahass, H. Zeyada, M. Aziz, N. El-Ghamaz, Structural and optical properties of thermally evaporated zinc phthalocyanine thin films, Opt. Mater. 27 (2004) 491–498.
[19] D. Dorranian, L. Dejam, G. Mosayebian, Optical characterization of Cu_3N thin film with Swanepoel method, J. Theor. Appl. Phys. 6 (2012) 13.
[20] E.G. Birgin, I. Chambouleyron, J.M. Martínez, Estimation of the optical constants and the thickness of thin films using unconstrained optimization, J. Comput. Phys. 151 (1999) 862–880.
[21] E.G. Birgin, I.E. Chambouleyron, J. Mario Martínez, Optimization problems in the estimation of parameters of thin films and the elimination of the influence of the substrate, J. Comput. Appl. Math. 152 (2003) 35–50.
[22] D.M. Roessler, Kramers-Kronig analysis of reflection data, Br. J. Appl. Phys. 16 (1965) 1119.
[23] Kramers-Kronig Relations and Sum Rules in Linear Optics, 110 (2005) 27-48.
[24] L.L. Kiang, Study on the optical properties of semiconductors by Kramers-Kronig transformation, Chin. J. Phys. 14 (1976) 93–100.
[25] S. Scheel, L. Knöll, D.G. Welsch, Spontaneous decay of an excited atom in an absorbing dielectric, Phys. Rev. A 60 (1999) 4094–4104.
[26] J. Tauc, R. Grigorovici, A. Vancu, Optical properties and electronic structure of amorphous germanium, physica status solidi, Phys. Status Solidi(b) 15 (1966) 627–637.
[27] M. Shkir, S. AlFaify, Tailoring the structural, morphological, optical and dielectric properties of lead iodide through Nd3+ doping, Sci. Rep. 7 (2017) 16091.
[28] M. Shkir, S. AlFaify, I.S. Yahia, V. Ganesh, H. Shoukry, Microwave-assisted synthesis of Gd3+ doped PbI2 hierarchical nanostructures for optoelectronic and radiation detection applications, Phys. B: Condens. Matter 508 (2017) 41–46.
[29] M. Shkir, S. AlFaify, I.S. Yahia, M.S. Hamdy, V. Ganesh, H. Algarni, Facile hydrothermal synthesis and characterization of cesium-doped PbI2 nanostructures for optoelectronic, radiation detection and photocatalytic applications, J. Nanopart. Res. 19 (2017) 328.
[30] M. Shkir, I.S. Yahia, V. Ganesh, H. Algarni, S. AlFaify, Facile hydrothermal-assisted synthesis of Gd3+ doped PbI2 nanostructures and their characterization, Mater. Lett. 176 (2016) 135–138.
[31] N.S. Das, P.K. Ghosh, M.K. Mitra, K.K. Chattopadhyay, Effect of film thickness on the energy band gap of nanocrystalline CdS thin films analyzed by spectroscopic ellipsometry, Phys. E: Low-Dimensional Syst. Nanostruct. 42 (2010) 2097–2102.
[32] M.M. Shehata, H. Kamal, H.M. Hasheme, M.M. El-Nahass, K. Abdelhady, Optical spectroscopy characterization of zinc tetra pyridel porphine (ZnTPyP) organic thin films, Opt. Laser Technol. 106 (2018) 136–144.
[33] P.L. Washington, H.C. Ong, J.Y. Dai, R.P.H. Chang, Determination of the optical constants of zinc oxide thin films by spectroscopic ellipsometry, Appl. Phys. Lett. 72 (1998) 3261–3263.
[34] A.B. Khatibani, S.M. Rozati, Optical and morphological investigation of aluminium and nickel oxide composite films deposited by spray pyrolysis method as a basis of solar thermal absorber, Bull. Mater. Sci. 38 (2015) 319–326.
[35] M. Shkir, V. Ganesh, S. AlFaify, I. Yahia, H. Zahran, Tailoring the linear and nonlinear optical properties of NiO thin films through Cr 3+ doping, J. Mater. Sci.: Mater. Electron. 29 (2018) 6446–6457.
[36] F. Bourguiba, A. Dhahri, T. Tahri, K. Taibi, J. Dhahri, E.K. Hlil, Structural, optical spectroscopy, optical conductivity and dielectric properties of $BaTi_{0.5}(Fe_{0.33}W_{0.17})O_3$ perovskite ceramic, B Mater. Sci. 39 (2016) 1765–1774.
[37] R.P.S.M. Lobo, 3 - The optical conductivity of high-temperature superconductors, High-Temperature Superconductors, Woodhead Publishing, 2011, pp. 103–146.
[38] H.S. Bolarinwa, M.U. Onuu, A.Y. Fasasi, S.O. Alayande, L.O. Animasahun, I.O. Abdulsalami, O.G. Fadodun, I.A. Egunjobi, Determination of optical parameters of zinc oxide nanofibre deposited by electrospinning technique, J. Taibah Univ. Sci. 11 (2017) 1245–1258.
[39] S. Gokhale, S.R. Barman, D.D. Sarma, Dielectric function and optical conductivity of TiO_x ($0.8 < x < 1.3$) determined from electron energy-loss spectroscopy, Phys. Rev. B 52 (1995) 14526–14530.
[40] W.N. Herman, S.R. Flom, S.H. Foulger, Organic Thin Films for Photonic Applications, American Chemical Society, 2010.
[41] M. Shkir, M. Taukeer Khan, V. Ganesh, I.S. Yahia, B. Ul Haq, A. Almohammedi, P.S. Patil, S.R. Maidur, S. AlFaify, Influence of Dy doping on key linear, nonlinear

and optical limiting characteristics of SnO2 films for optoelectronic and laser applications, Opt. Laser Technol. 108 (2018) 609–618.
[42] M. Frumar, J. Jedelský, B. Frumarová, T. Wágner, M. Hrdlička, Optically and thermally induced changes of structure, linear and non-linear optical properties of chalcogenides thin films, J. Non-Cryst. Solids 326–327 (2003) 399–404.
[43] J. Xia, Y. Liu, X. Qiu, Y. Mao, J. He, L. Chen, Solvothermal synthesis of nanostructured $CuInS_2$ thin films on FTO substrates and their photoelectrochemical properties, Mater. Chem. Phys. 136 (2012) 823–830.
[44] H. Ticha, L. Tichy, Semiempirical relation between non-linear susceptibility (refractive index), linear refractive index and optical gap and its application to amorphous chalcogenides, J. Optoelectron. Adv. Mater 4 (2002) 381–386.
[45] R. Adair, L.L. Chase, S.A. Payne, Nonlinear refractive index of optical crystals, Phys. Rev. B 39 (1989) 3337–3350.
[46] V. Ganesh, M. Shkir, S. AlFaify, I.S. Yahia, H.Y. Zahran, A.F.A. El-Rehim, Study on structural, linear and nonlinear optical properties of spin coated N doped CdO thin films for optoelectronic applications, J. Mol. Struct. 1150 (2017) 523–530.
[47] M. Shkir, M. Arif, V. Ganesh, M.A. Manthrammel, A. Singh, I.S. Yahia, S.R. Maidur, P.S. Patil, S. AlFaify, Investigation on structural, linear, nonlinear and optical limiting properties of sol-gel derived nanocrystalline Mg doped ZnO thin films for optoelectronic applications, J. Mol. Struct. 1173 (2018) 375–384.
[48] L.G. Holmen, M.W. Haakestad, Optical limiting properties and z-scan measurements of carbon disulfide at 2.05 μm wavelength, JOSA B 33 (2016) 1655–1660.
[49] P. Poornesh, P.K. Hegde, G. Umesh, M. Manjunatha, K. Manjunatha, A. Adhikari, Nonlinear optical and optical power limiting studies on a new thiophene-based conjugated polymer in solution and solid PMMA matrix, Opt. Laser Technol. 42 (2010) 230–236.